ACS OMEGA

Open Access



http://pubs.acs.org/journal/acsodf

Article

# Is Fe the Most Active Site for Fe/N-Doped Graphdiyne?

Yuanyi Feng, Mingying Sun, Yongfei Ji,* and Ting Fan*

Cite This: *ACS Omega* 2024, 9, 17389−17397

Read Online

ACCESS | Metrics & More | Article Recommendations | Supporting Information

**ABSTRACT:** We performed a systematic study on the activity of pristine, Fe-doped, N-doped, and Fe/N-codoped graphdiyne (GDY) for oxygen reduction reactions (ORRs). We found that the pristine GDY has a high overpotential because of the weak binding of the intermediates. The sp-hybridized N-doped GDY enhances the binding of the intermediates at the adjacent sp-hybridized C site, which greatly enhances its ORR activities with a low overpotential of 0.45 V. On the other hand, on Fe-doped GDY, the binding of the intermediates at the Fe site and its neighboring C sites becomes too strong, while the C site at the second nearest acetylene chain becomes the most active site with an overpotential of 0.43 V. In the case of Fe and N codoping, Fe and the C sites near Fe and N still bind the intermediates too strongly, and the most active site is located at the C with an optimal distance. The binding energy of OH* is an activity descriptor for Fe- and/or N-doped GDY. Based on the machine learning analysis of $\Delta G(OH^*)$, both the properties of the active center (electronic and geometric properties) and its environment, especially the latter, play important roles in determining its activity. The scaling relation analysis and volcano plot suggest that Fe and N doping enhance the binding of the intermediates to different extents, and the C atom, which is bonded neither to N nor to Fe atom, with an optimal binding strength, becomes the most active site.

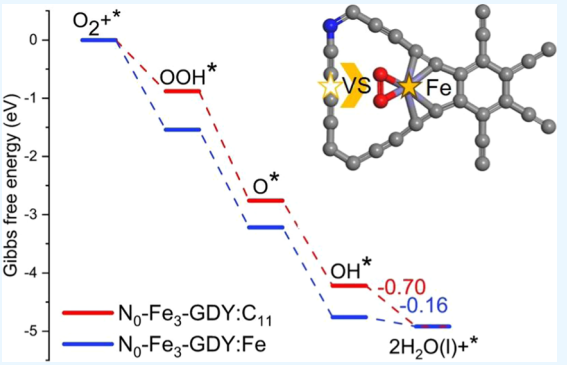


## INTRODUCTION

Due to the growing energy crisis, it is urgent to develop alternate sources of energy and clean energy conversion devices. Hydrogen is one of the shining stars of clean energy. One way that hydrogen can be used for energy conversion is a proton-exchange membrane (PEM) fuel cell, in which hydrogen is oxidized at the anode and oxygen is reduced at the cathode. That is, the cathodic oxygen reduction reaction (ORR) is a key step that limits the energy conversion efficiency and the bottleneck of PEM fuel cells owing to the sluggish kinetics. Currently, noble-metal-based catalysts (for example, platinum, iridium, and palladium) have long been regarded as the most efficient catalysts for ORR, with Pt/C performing the best. However, the prohibitive cost limits the large-scale commercial application of PEM fuel cells and other renewable energy technologies. Therefore, it is imperative and desirable to search for inexpensive, durable, and active alternatives. One way is to improve the utilization efficiency of noble metals such as single-atom catalysts. In addition, downsizing bulk metals to single-atom catalysts (SAC) could significantly change the catalytic behaviors of the metal catalysts, benefiting the electrocatalytic process.[1,2]

Graphdiyne (GDY), a novel allotrope of two-dimensional carbon materials, is expected to be a good support to anchor single-atom catalysts.[3] Different from graphene consisting of only $sp^2$-hybridized carbon atoms, GDY contains both $sp^2$- and sp-hybridized carbon atoms.[4] The coexistence of sp and $sp^2$ carbons makes an uneven charge distribution of carbon atoms, which helps stabilize metal atoms and facilitate $O_2$ adsorption. More importantly, GDY sheets possess uniformly distributed pores surrounded by sp-hybridized carbon atoms, not only ensuring a wide specific surface area but also supplying stable binding sites to anchor metal atoms. Thus, GDY-based materials have emerged as promising electrocatalytic catalysts.[5−12]

The group of Wang and Li found that the ORR reduction performance of sp-N-doped GDY (N-GDY) was greatly improved compared to pristine GDY and comparable to that of commercial Pt/C under alkaline conditions.[13] Graphdiyne-supported single-atom-sized Fe catalysts (Fe-GDY) are synthesized by Cai and co-workers. Also, Fe-GDY shows high catalytic activity to ORR, similar to commercial Pt/C in alkaline electrolytes.[14] Later, Huang's group successfully synthesized Fe/N-doped graphdiyne (Fe,N-GDY), which shows similar or even higher onset potential with the Pt/C catalyst but higher stability and excellent resistance to methanol poisoning.[15,16] Comparing the performance of Fe,N-GDY, Fe-GDY, and N-GDY, they found that the performance of the codoped catalysts was greater than that

Received: January 4, 2024
Revised: March 20, 2024
Accepted: March 22, 2024
Published: April 3, 2024

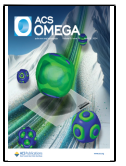





https://doi.org/10.1021/acsomega.4c00093
*ACS Omega* 2024, 9, 17389−17397

of the single-doped catalysts. However, the performance of Fe-GDY and N-GDY synthesized by Huang's group is lower than that of Fe-GDY synthesized by Cai's group and that of N-GDY synthesized by the group of Wang and Li. This should come from different synthesis methods leading to N substitution at different positions of GDY or different forms of Fe.

Because the forms of N-GDY, Fe-GDY, and Fe,N-GDY are tremendous, it is impossible to investigate all of the forms. We only consider the form with one N and one Fe substitution in this paper to probe whether Fe,N-GDY improves the catalytical activity to ORR compared to N-GDY and Fe-GDY. In 2019, Du's group theoretically investigated transition-metal single-atom doped GDY for water oxidation (oxygen evolution reaction, OER).[5] As the ORR is the reverse reaction of the OER, the overpotential of Fe-GDY to ORR is 1.27 V based on its OER results. The high overpotential contradicts the high catalytic activity of Fe-GDY for ORR. This should come from two reasons. One is that they use the wrong structure of Fe-GDY in the calculation. Thorough X-ray absorption near edge structure (XANES) analysis shows that the structure of Fe,N-graphene, its analogy, possesses an oxygen molecule in the side-on mode or two oxygen molecules in the end-on mode.[17] No matter whether the oxygen molecule is in the side-on or end-on mode, the coordination number is 6. In addition, our recent study found that the coadsorbed $O_2$ greatly improves the performance of graphdiyne-supported single-atom cobalt catalyst for ORR. X-ray photoelectron spectrum (XPS) of Fe,N-GDY in Huang's paper manifests that the oxygen-containing functional group should be the coordination atom of Fe, and the coordination number is approximately 6 based on extended X-ray absorption fine structure (EXAFS) fitting.[16] Thus, there should be adsorbates on Fe-GDY and Fe,N-GDY. The other reason is that Fe is not the most active site. In Du's study, they only consider Fe as the active site. Maybe carbon is also the active site. For N-GDY, the doping N will induce a partial positive charge on the adjacent carbon atoms, which are the most active sites for N-GDY.[18,19] Similarly, the doping Fe can also change the charge distribution of carbon atoms,[20] and thus carbon can also be the active site.[21] In addition, partial poisoning was observed in Fe,N-GDY by adding KSCN,[15,16] which indicates that Fe is not the only active site.

To this end, we will present a theoretical study on the ORR catalytic activity of Fe,N-GDY compared to N-GDY and Fe-GDY, considering adsorbates and Fe as well as C as active sites. Through calculations, we hope to unveil whether Fe is the most active site and the synergistic effect of Fe and N.

## COMPUTATIONAL METHODS

All density functional calculations presented were performed with Vienna ab initio simulation package (VASP)[22] at the spin-polarized generalized gradient approximation (GGA) level. The PBE functional with the projector-augmented wave (PAW) pseudopotential was adopted. DFT-D3 method with Becke−Jonson damping was used to consider van der Waals interactions. An energy cutoff of 460 eV was applied. The solvent effect was included with VASPsol with water as the solvent. The DFT + $U$ method was used with $U - J = 3.29$ for Fe. Graphdiyne was presented by a 2 × 2 supercell of a monolayer slab with a vacuum layer of 14 Å. The energies and residual forces were converged to $10^{-5}$ eV and 0.02 eV/Å during optimizations, respectively. The Monkhorst-pack grid $k$-points[23] of 1 × 1 × 1 was applied during optimization, and 2 × 2 × 1 was used for the single-point calculation to refine the electronic energy. Table S1 shows the $k$-point test for some selected structures.

For the model of N-GDY, Fe-GDY, and Fe,N-GDY, we only consider one N and one Fe substitution in this paper, as mentioned in the Introduction. As adsorbates can change the catalytic activity, the real catalyst should be adsorbates binding to Fe-GDY and Fe,N-GDY. Based on the XANES analysis of Fe,N-graphene and the EXAFS of Fe,N-GDY, the coordination number is 6. In addition, the XPS spectrum of Fe,N-GDY in Huang's paper manifests the oxygen-containing functional group. The oxygen-containing functional group could be $O_2$, OOH, O, and OH.[24,25] For ORR, the rate-determining step could be either the first step or the last step.[26] Thus, the most possible adsorbates are $O_2$ or OH. The Fe-GDY and Fe,N-GDY with an oxygen molecule in the side-on mode are the models we used to investigate the whole energy surface.[27] The ORR activity was further tested at Fe and some selected carbon atoms on the model of Fe-GDY and Fe,N-GDY with two binding OH atoms or two binding end-on $O_2$. To figure out if Fe is the most active site for Fe-GDY and Fe,N-GDY, we screened all of the sp-hybridized carbon atoms in the acetylenic-like rods and the Fe atom to calculate the adsorption of the ORR intermediates and the free energy diagrams on these possible sites. To analyze whether Fe and N have synergistic effects, their partial density of states (PDOS) was analyzed by DS-PAW.[28]

To analyze the stability of Fe-GDY and Fe,N-GDY, the binding energy ($E_b$) was calculated as

$$E_b = E_{X\text{-}GDY} - E_C - E_X$$

where $E_{X\text{-}GDY}$ is the energy of X-doped GDY, such as Fe-GDY or Fe,N-GDY, $E_C$ is the energy of the corresponding X-doped GDY without X atom, and $E_x$ is the energy of X bulk per atom.

The overall 4e$^-$ ORR process in an acidic medium can be described as

$$O_2 + 4e^- + 4H^+ \rightarrow 2H_2O$$

The possible reaction pathways are as follows:

$$^*+O_2 + e^- + H^+ \rightarrow OOH^*, \quad \Delta G_1$$

$$OOH^* + e^- + H^+ \rightarrow H_2O + O^*, \quad \Delta G_2$$

$$O^* + e^- + H^+ \rightarrow OH^*, \quad \Delta G_3$$

$$OH^* + e^- + H^+ \rightarrow H_2O + ^*, \quad \Delta G_4$$

where O*, OH*, and OOH* are adsorbed intermediates. The free energy changes for each elementary step can be calculated based on the computational hydrogen electrode (CHE) model developed by Nørskov et al. The energy of the ($H^+ + e^-$) pair is related to the energy of $H_2$ (gas) and applied potential ($U$). Thus, the free energy changes, for example, step 1, can be described as

$$\Delta G_1 = G_{OOH*} - G_{O_2} - \frac{1}{2}G_{H_2} + eU$$

In the present work, the reaction conditions of $U = 0$, pH = 0, and $T = 298.15$ K are applied. The free energy of $H_2O$ (l) is calculated with a gas-phase $H_2O$ molecule at 3534 Pa. Since the energy of $O_2$ is poorly described by density functional



https://doi.org/10.1021/acsomega.4c00093
ACS Omega 2024, 9, 17389−17397

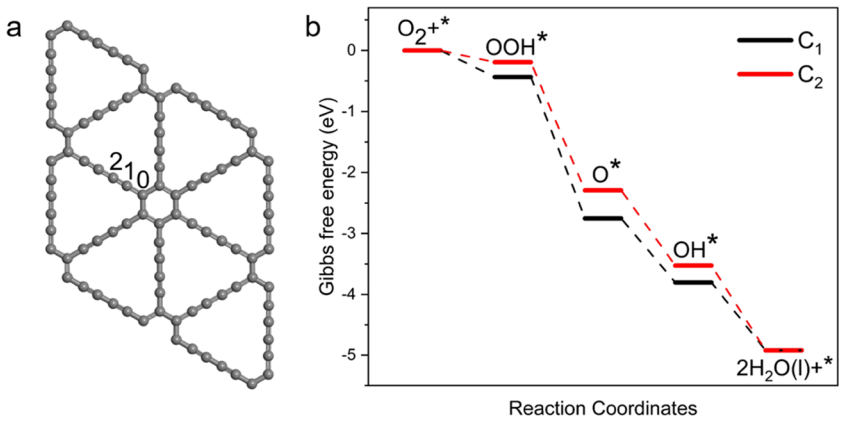


**Figure 1.** Structure and atomic ordering diagrams of (a) GDY and (b) calculated free energy diagrams of GDY (asterisk "*" represents the substrate GDY).

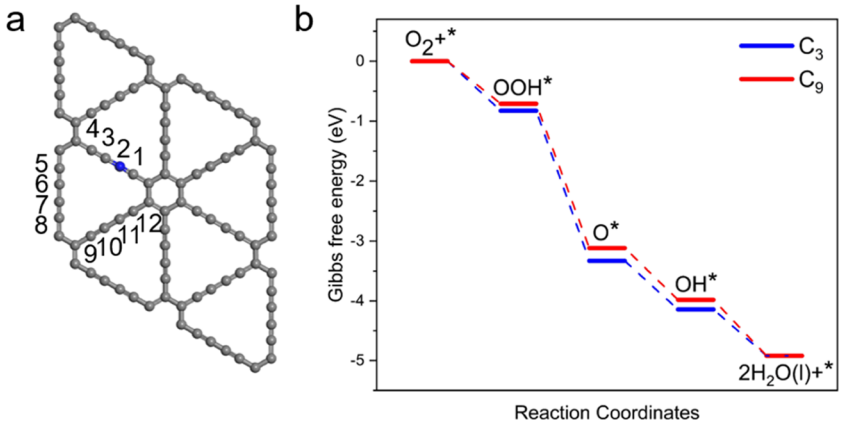


**Figure 2.** Structure and atomic ordering diagrams of (a) $N_2$-GDY and (b) calculated free energy diagrams of $N_2$-GDY (asterisk "*" represents the substrate $N_2$-GDY).

theory (DFT), the free energy of $O_2$ is calculated as $\Delta G_{O_2} = 4.92 + 2G_{H_2O} - 2G_{H_2}$.

The step with the lowest $\Delta G$ is the rate-determining step, which determines the onset potential:

$$U_{onset} = -\min[\Delta G_1, \Delta G_2, \Delta G_3, \Delta G_4]/e$$

Then, the overpotential is

$$\eta = 1.23 - U_{onset}$$

## RESULTS AND DISCUSSION

**ORR Catalyzed by GDY and N-GDY.** For GDY, three active sites are calculated because of its symmetry. The detailed energies are shown in Table S2. The $C_0$ site is inactive for the ORR and therefore is not considered in other structures. Figure 1 shows the Gibbs reaction free energy of $C_1$ and $C_2$. $C_1$ is more active than $C_2$. The overpotential of $C_1$ is 0.80 V. For N-GDY, there are three positions for N doping, as shown in Figure 1a. ORR activity on the doped chain and the undoped chains in the triangle area are all investigated. To evaluate the stability of N-GDY, the formation energy is computed via the equation: $E_f = E_{N\text{-}GDY} - E_{GDY} - \mu_C + \mu_N$, where $\mu_C$ and $\mu_N$ are the energies of pristine graphdiyne and nitrogen bulk per atom, respectively. The formation energy of $N_0$-GDY, $N_1$-GDY, and $N_2$-GDY are 1.47, 0.38, and 0.68 eV, respectively. Based on previous work, N doping at the $C_2$ position can endow GDY with the highest ORR activity as experimentally obtained.[18,29] However, they did not consider the ORR activity on the undoped chains. Our calculations show that not only the doped chain but also the undoped chains are active for ORR. The Gibbs reaction free energy of each intermediate and each elementary step and the overpotential on the active sites are shown in Table S3. $N_0$-GDY, $N_1$-GDY, and $N_2$-GDY show a similar onset potential, which is about 0.70 V. $N_2$-GDY shows the highest ORR activity. Figure 2 shows the detailed free energy profiles of the two most active sites at $N_2$-GDY. The calculated rate-determining step (RDS) is the fourth step for $C_3$, the reduction of OH* to $H_2O$, while the first step for $C_9$ is the reduction of $O_2$ to OOH*. The overpotentials are 0.45 and 0.52 V for $C_3$ and $C_9$, respectively. The overpotential is 0.45 V, which is comparable to the experimental value of about 0.5 V in an acidic condition[13] and others' calculation results.[18,29]

**ORR Catalyzed by Fe-GDY.** For Fe-GDY, it is found that the supported Fe atom is very stable at the corner of the acetylene, as shown in Figure 3a. As aforementioned, we used Fe-GDY binding with a side-on $O_2$ molecule as a model to calculate its ORR performance, its optimized structure is shown in Figure 3b. The model is labeled as Fe−$O_2$s-GDY, of which s stands for side-on. Given the symmetric structure of Fe−$O_2$s-GDY, only $C_1$−$C_4$ are searched for the possible carbon active sites for the doped chains and $C_5$−$C_8$ for the undoped chain. The Gibbs reaction free energy of each intermediate and each elementary step and the overpotential


https://doi.org/10.1021/acsomega.4c00093
ACS Omega 2024, 9, 17389−17397

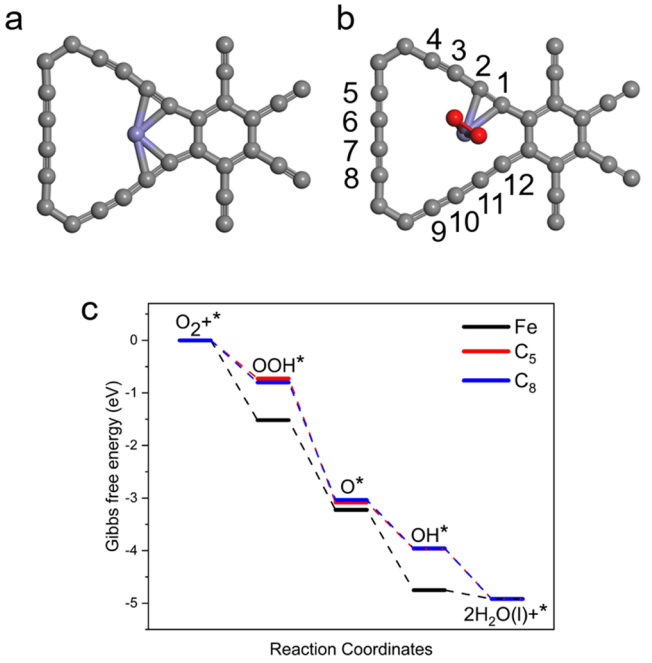


**Figure 3.** Structure and atomic ordering diagrams of (a) Fe-GDY and (b) Fe−$O_2$s-GDY. (c) Calculated free energy diagrams of Fe−$O_2$s-GDY (asterisk "*" represents the substrate Fe−$O_2$s-GDY).

on the active sites are listed in Table S4. It was found that carbon sites on the doped chain are not more active than those on the undoped chain. Their detailed Gibbs reaction free energies of the two most active carbon sites and Fe site are shown in Figure 3c. When Fe is the active site, the RDS is the fourth step, and the overpotential is 1.06 V, which is lower than 1.27 V in Du's study. This indicates that coadsorbed $O_2$ greatly improves the performance of Fe-GDY. When carbons are the active sites, their overpotentials are 0.50 and 0.43 V for $C_5$ and $C_8$, respectively. Comparing the overpotentials at Fe, $C_5$, and $C_8$, $C_5$ and $C_8$ are much more active than Fe, which suggests that Fe is not the most active site for Fe-GDY.

**ORR Catalyzed by Fe,N-GDY.** For Fe,N-GDY, there are three doping positions for N and three anchoring positions available for Fe. In order to fully investigate the effect of doping sites of N and Fe on the ORR activity, nine possible configurations for a single Fe atom anchored on N-doped GDY were constructed, labeled as $N_xFe_y$ (Figure 4). The subscript of N indicates its doping position of GDY, the same as in Figure 1a, while the subscript of Fe indicates its relative position to N, where the corner of the acetylenic closest to N is defined as $Fe_1$, as shown in Figure 4a. The ordinal number $y$ increases counterclockwise, causing $Fe_3$ to be located in the corner farthest away from N, as can be seen from their abbreviations labeled in Figure 4. The relative energies of these nine possible configurations of Fe,N-GDY are given in Table S5.

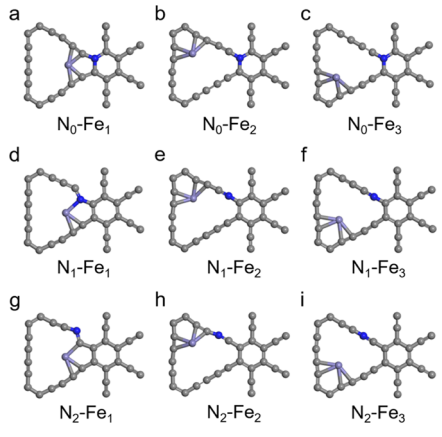


**Figure 4.** Structures of nine possible configurations of Fe,N-GDY.

To investigate Fe,N-GDY comprehensively, the most stable and least stable Fe,N-GDY were chosen for further calculations, denoted as $N_1$−$Fe_2$ and $N_0$−$Fe_3$. Their binding energies are listed in Table S6, and it can be seen that the binding energy of Fe,N-GDY is lower than that of Fe-GDY, indicating the doping of N helps to anchor the Fe atom.[30,31]

The optimized structures and ordering of $N_1$−$Fe_2$ and $N_0$−$Fe_3$ with a side-on $O_2$ are shown in Figure 5. All possible active sites are searched. The Gibbs reaction free energy of each intermediate and each step and the overpotential on the active sites are shown in Table S7. The calculated free energy diagrams of Fe as the active site and some selected carbon sites with the highest or similar ORR activities are shown in Figure 5. For $N_1$−$Fe_2$, the most active sites are Fe, $C_9$, and $C_{12}$. The lowest overpotential of $N_1$−$Fe_2$ is located at $C_9$ with 0.54 V, and that of the Fe site is 0.60 V. Comparing $N_1$-GDY, $C_9$ is the most active carbon site for both $N_1$-GDY and $N_1$−$Fe_2$. In addition, their overpotentials at $C_9$ are similar, and the overpotential for $N_1$−$Fe_2$ is a little lower than that for $N_1$-GDY (0.60 V). For $N_0$−$Fe_3$, the most active sites are $C_2$ and $C_{11}$, not Fe. Also, the overpotential of $N_0$−$Fe_3$ at $C_2$ and $C_{11}$ is 0.55 V and 0.53 V, much lower than that of the Fe site (1.07 V).

The overpotentials of the Fe site of Fe-GDY and $N_0$−$Fe_3$ are almost the same, which are 1.06 and 1.07 V, higher than that of $N_1$−$Fe_2$ (0.60 V). Comparing the adsorption energy of OOH*, O*, and OH* at the Fe site, it was found that the adsorption energy is also quite similar between Fe-GDY and $N_0$-$Fe_3$, lower than that on $N_1$−$Fe_2$. Figure 6 shows the PDOS of the N and Fe atoms of $N_1$−$Fe_2$ and $N_0$−$Fe_3$. In $N_1$−$Fe_2$, the N atom interacts with the neighboring carbon atom $C_2$, which indirectly interacts with $C_3$ and the Fe atom. It clearly shows the far-away N atom has a much weaker interaction with the Fe atom in $N_0$−$Fe_3$. In addition, the binding energy of $N_0$−$Fe_3$ and Fe-GDY is 4.06 and 4.12 eV, higher than that of $N_1$−$Fe_2$ (3.57 eV), shown in Table S6. This also indicates that the interaction between N and Fe is weaker and similar in $N_0$−$Fe_3$ and Fe-GDY compared to that in $N_1$−$Fe_2$.

**Scaling Relations, Volcano Plots, and Origin of ORR Activity Trend.** We explore the scaling relation among the Gibbs reaction free energies of OOH*, O*, and OH* at all possible active sites of Fe−$O_2$s-GDY and Fe−$O_2$s-N-GDY, as shown in Figure 7a,b. The best linear fit obtained for Fe/N-doped GDY is $\Delta G_{OOH^*} = 0.83\ \Delta G_{OH^*} + 2.64$ ($R^2 = 0.87$) and $\Delta G_{O^*} = 1.17\ \Delta G_{OH^*} + 1.63$ ($R^2 = 0.86$). This scaling relationship indicates a strong linear correlation between $\Delta G_{OOH^*}$, $\Delta G_{O^*}$, and $\Delta G_{OH^*}$. Typically, the RDS of the ORR process is the first step or the fourth step.[26,32−34] This is also the case for our system. Based on these findings, we used the Gibbs reaction free energy of OH* ($\Delta G_{OH^*}$) as a descriptor of ORR catalytic performance at different active sites on Fe/N-doped GDY surfaces, as shown in Figure 7c,d. The vertical coordinate is the negative overpotential calculated from the first step or the fourth step, and the horizontal coordinate is $\Delta G_{OH^*}$, constituting the ORR activity volcano plot of Fe/N-doped GDY.



https://doi.org/10.1021/acsomega.4c00093
ACS Omega 2024, 9, 17389−17397

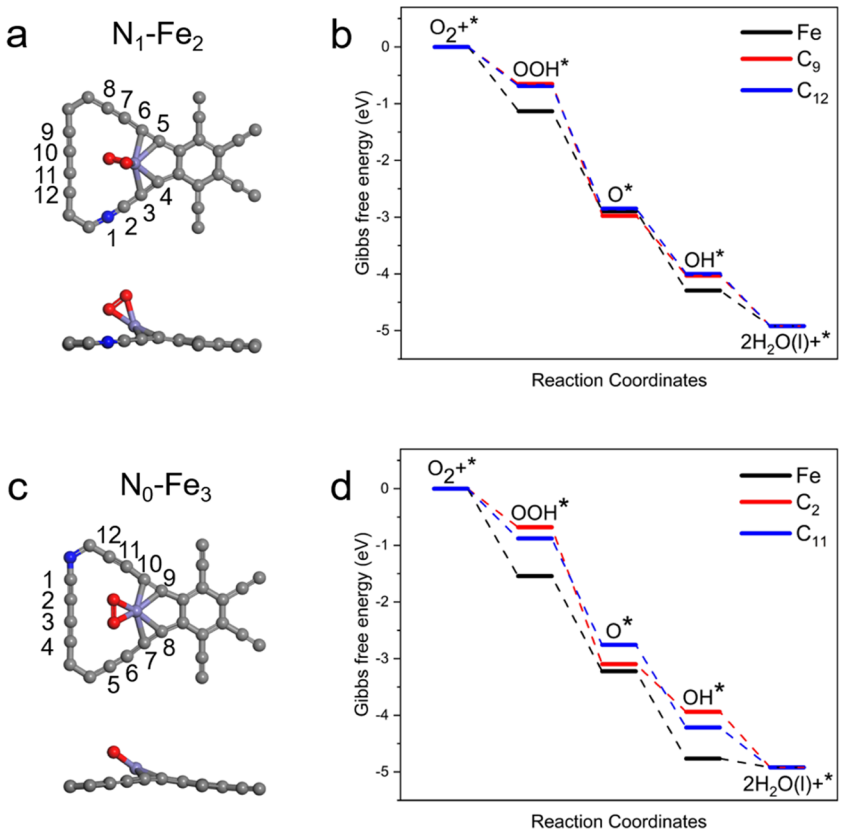


**Figure 5.** Structure and atomic ordering diagrams of (a) $N_1$−$Fe_2$ and (b) calculated free energy diagrams of $N_1$−$Fe_2$ and structure and atomic ordering diagrams of (c) $N_0$−$Fe_3$ and (d) calculated free energy diagrams of $N_0$−$Fe_3$ (asterisk "*" represents the substrates N−Fe−$O_{2s}$-GDY).

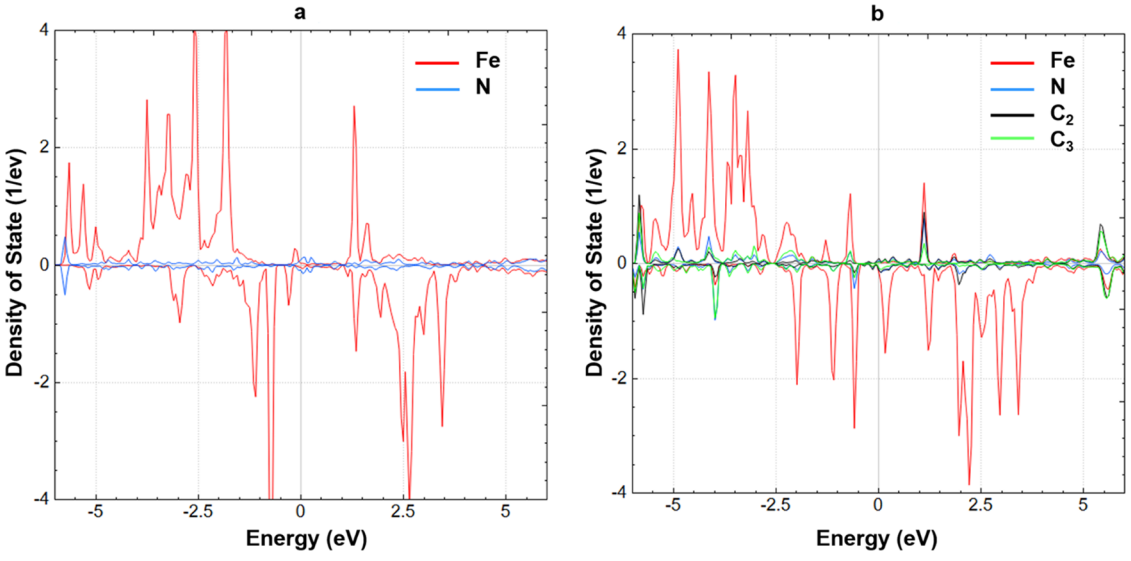


**Figure 6.** Calculated projected density of state (PDOS) of (a) $N_0$-$Fe_3$−$O_2$s-GDY and (b) $N_1$-$Fe_2$−$O_2$s-GDY.

As can be seen in Figure 7c, all of the Fe sites are located at the left branch of the volcano, which means too strong adsorption of OH*, and the rate-determining step is the reduction of OH*. In addition, it clearly shows that the Fe site is not the most active compared to carbon sites. The majority of active sites of N-GDY (the black label) are located at the right branch of the volcano plot, indicating that the RDS of ORR is mainly the reduction of $O_2$ and too weak adsorption of OH*. The active sites of Fe,N-GDY (the red and blue labels) are scattered on both sides of the volcano. Comparing the adsorption energy of OH* among GDY, N-GDY, and Fe-GDY (Figure 8), it was found that either N doping or Fe doping would strengthen the binding of OH. Table S8 shows the change of Bader charge of N or Fe−$O_{2S}$ is both positive when the OH is adsorbed, indicating that Fe or N is N-type doping and thus strengthens the binding of OH. Comparing the adsorption energy of OH* between N-GDY/Fe-GDY and Fe,N-GDY, there is no clear trend, as OH binds strongly at some sites and weakly at the other sites (Figure S1).



https://doi.org/10.1021/acsomega.4c00093
ACS Omega 2024, 9, 17389−17397

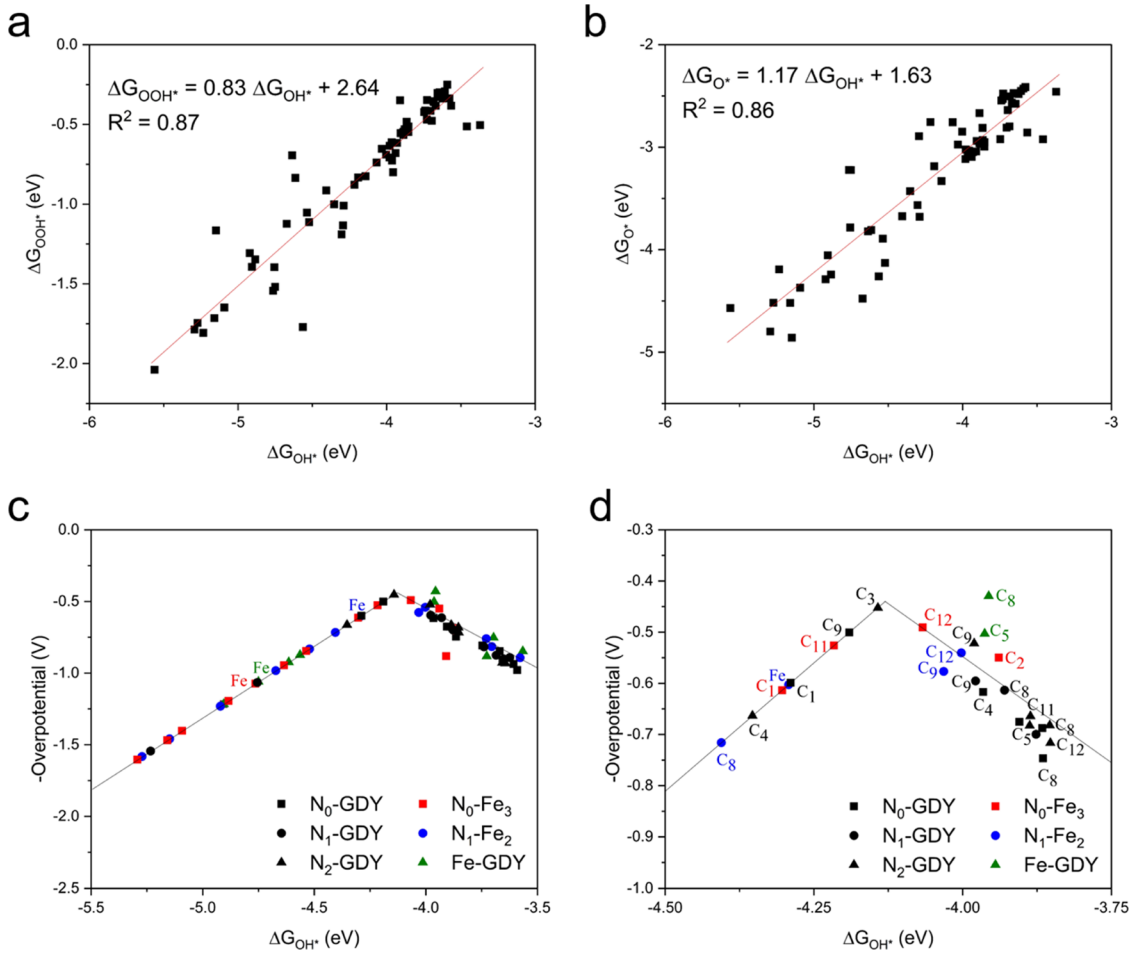


**Figure 7.** (a) Gibbs reaction free energies of OOH* plotted against the Gibbs reaction free energies of OH*. (b) Gibbs reaction free energies of O* plotted against the Gibbs reaction free energies of OH*. (c) Activity volcano plot for ORR showing the negative overpotential as a function of the Gibbs reaction free energies of OH* on all active sites of Fe−$O_2$s-GDY and Fe−$O_2$s-N-GDY. (d) Activity volcano plot of $\Delta G_{OH^*}$ in the range of −4.50 and −3.75 eV.

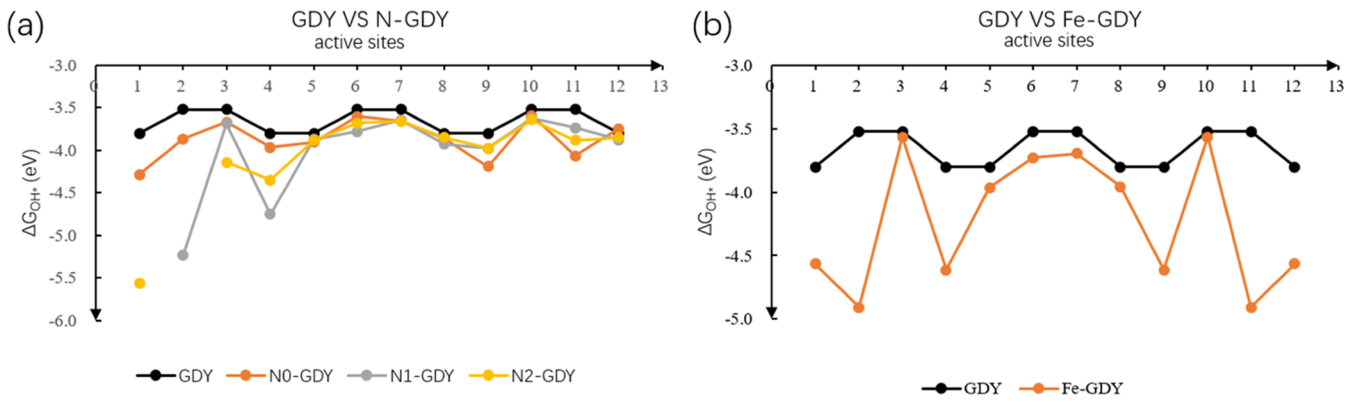


**Figure 8.** Comparison of $\Delta G_{OH^*}$ (a) between GDY and N-GDY and (b) between GDY and Fe-GDY at the corresponding sites.

To probe the trending of codoping of Fe and N, we performed a machine learning analysis on the $\Delta G$(OH*) with the Gradient Boost Regression (GBR) algorithm[35,36] because it is less likely to overfit the data.[37] Several electronic and geometric features of the active site are included as the features, which include the p-band center (pbc), Bader charge, magnetic moment (mag), and average distance with adjacent atoms (d_ave); dd is the sum of $r_{ab} - (r_a + r_b)$ over all the bonds the C atom take parts in ($r_{ab}$ is the bond length between atom a and b, and $r_a$, $r_b$ are the radii of atoms a and b). To take into account the different coordination environments, we have also included the coordination number (Nc), the sum of the neighboring atoms' Pauli electronegative (s-P),[38] the sum of the neighboring atoms' first ionization energy (s-I), the distance to the Fe atom (dCFe), and the distance to the N atom (dCN). A full list of the features can be found in the Supporting Information (Table S9). As shown in Figure 9a, the GBR-predicted $\Delta G$(OH*) agrees well with the DFT-


https://doi.org/10.1021/acsomega.4c00093
ACS Omega 2024, 9, 17389−17397

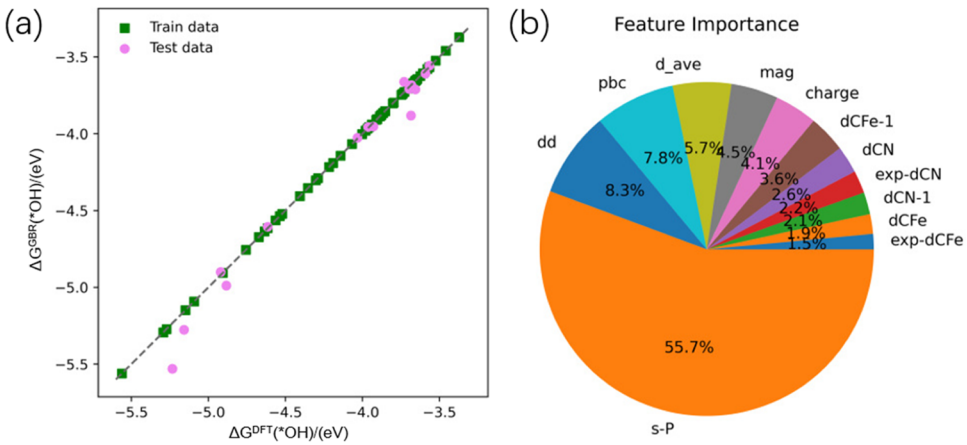


**Figure 9.** (a) $\Delta G$(OH*) from DFT calculation versus machine learning predicted values. (b) Feature importance, the full list, and the meaning of the feature can be found in Table S7.

**Table 1. Gibbs Reaction Free Energy Changes ($\Delta G$) of OH* and Overpotentials ($\eta$) of the Most Active Carbon Sites and Fe Sites of GDY, N-GDY, Fe-GDY, and Fe,N-GDY**

| | | $\Delta G_{OH*}$ (eV) | $\eta$ (V) | | | $\Delta G_{OH*}$ (eV) | $\eta$ (V) |
|---|---|---|---|---|---|---|---|
| GDY | $C_1$ | −3.80 | 0.80 | Fe-GDY | Fe | −4.75 | 1.06 |
| $N_0$-GDY | $C_9$ | −4.19 | 0.50 | | $C_5$ | −3.96 | 0.50 |
| | $C_{11}$ | −4.07 | 0.49 | | $C_8$ | −3.96 | 0.43 |
| $N_1$-GDY | $C_8$ | −3.93 | 0.61 | $N_1$-$Fe_2$ | Fe | −4.29 | 0.60 |
| | $C_9$ | −3.98 | 0.60 | | $C_9$ | −4.03 | 0.58 |
| | | | | | $C_{12}$ | −4.00 | 0.54 |
| $N_2$-GDY | $C_3$ | −4.14 | 0.45 | $N_0$-$Fe_3$ | Fe | −4.76 | 1.07 |
| | $C_9$ | −3.98 | 0.52 | | $C_2$ | −3.94 | 0.55 |
| | | | | | $C_{11}$ | −4.22 | 0.53 |

calculated ones. The linear fitting between them presents an $R^2$ of 0.97 with a mean square error (MSE) of 0.01 eV. The leave-one-out cross-validation and the 10-fold repeated cross-validation were also employed to avoid overfitting. Both methods delivered a low mean average error (MAE) of 0.16 eV, which is superior to the performance of the GBR model on other systems.[37−40] Feature importance is shown in Figure 9b, and the most important feature is s-P, which suggests that the electronegativities of the neighboring atoms are very important, probably because they represent the availability of electrons from neighboring atoms, which is important for stabilizing the oxygen species. The sum of the feature importance of the electronic features (pbc, mag, and charge) is about 16.4%, which is comparable to the sum of dd and d_ave and also the sum of the features regarding the distance between C and N/Fe. Therefore, both the properties of the active center (electronic and geometric properties) and its environment, especially the latter, play important roles in determining its activity.

Table 1 summarizes the $\Delta G_{OH*}$ and overpotentials of the most active sites of GDY, N-GDY, Fe-GDY, and Fe,N-GDY. For Fe-GDY and Fe,N-GDY, Fe is not the only and most active site, which indicates partial poisoning in Fe,N-GDY by adding KSCN observed in the experiment.[15,16] In addition, doping GDY with one N or one Fe atom can greatly reduce its overpotential. However, codoping GDY with one N and one Fe atom has comparable overpotentials with N-GDY and Fe-GDY. Based on the binding energies of Fe-GDY and Fe,N-GDY in Table S6, the Fe atom binds strongly when GDY is doped with N except $N_1$−$Fe_1$. Although codoping does not improve the ORR activity of GDY compared to N-GDY and Fe-GDY, N doping improves the stability of Fe-GDY.

**Effects of Different Adsorbates.** As mentioned in the Computational Details section, the oxygen-containing functional group could be $O_2$, OOH, O, and OH. For ORR, the rate-determining step could be either the first step or the last step.[26] Thus, the most possible adsorbates are $O_2$ or OH. To probe whether OH or end-on $O_2$ will affect the conclusion that Fe is not the most active site, we calculated the Gibbs reaction free energies of each intermediate and each step and the overpotentials of some selected C sites and Fe sites. Table S10 shows the negative adsorption energies of $O_2$ and OH on Fe, which indicates that these adsorptions occur spontaneously. Fe-GDY or Fe,N-GDYs with two end-on $O_2$ are less stable than their corresponding structures with two side-on $O_2$, shown in Table S11. The optimized structures are shown in Figures S2 and S3. In addition, during optimization, the end-on $O_2$ will easily be turned into the side-on mode or the end-on $O_2$ will react with carbons on the GDY chains. Thus, Fe-GDY and Fe,N-GDY with two end-on $O_2$ are not discussed further. As for the OH ligand, the optimized structures are shown in Figure S4, and the corresponding Gibbs reaction free energies are shown in Table S12. It can be seen that all selected C sites are more active than the Fe site except the $C_2$ site of $N_0$-$Fe_3$ as the H atom of the ORR intermediate OH* will be transferred to the OH ligand of Fe, leading to a stronger adsorption.

In conclusion, regardless of the absorbates, the ORR catalytic activity of some selected C sites is still better than that of the Fe site, which proves that Fe is not the only and most active site for Fe/N-doped GDY.



https://doi.org/10.1021/acsomega.4c00093
ACS Omega 2024, 9, 17389−17397

## CONCLUSIONS

In summary, we have systematically investigated the activity of the Fe- and/or N-doped GDY for oxygen reduction reactions. We found that pristine GDY binds the intermediates too weakly, which results in high overpotentials. Fe or N doping greatly enhances the binding of the intermediates at multiple carbon sites. The most active site of N-doped GDY is the $C_3$ site for $N_2$-GDY, and that on Fe-GDY is the C site on the second nearest acetylene chain and not on the Fe site. In the case of Fe/N codoping, the most active C on Fe/N-codoped GDY is directly bonded neither to the N nor to the Fe atom; the far-away C site with an optimal binding strength becomes the most active site. The binding energy of OH* is an activity descriptor for Fe and/or N-doped GDY. Based on machine learning analysis on the $\Delta G$(OH*), both the properties of the active center (electronic and geometric properties) and its environment, especially the latter, play important roles in determining its activity. Although codoping does not improve the ORR activity of GDY compared to N-GDY and Fe-GDY, N doping improves the stability of Fe-GDY.

## ASSOCIATED CONTENT

### Supporting Information

The Supporting Information is available free of charge at https://pubs.acs.org/doi/10.1021/acsomega.4c00093.

The K-POINTS tests, the Gibbs reaction free energy changes ($\Delta G$) of ORR intermediates and elementary step and overpotential ($\eta$) of the active sites on N-GDY, Fe-GDY, and Fe,N-GDY, some optimized structures, full list of machine learning features, and relative energies of Fe-GDY and Fe,N-GDY with side-on or end-on $O_2$ (PDF)

## AUTHOR INFORMATION


### Corresponding Authors

**Ting Fan** − *School of Chemistry and Chemical Engineering, South China University of Technology, Guangzhou 510641, P. R. China;* orcid.org/0000-0001-9710-9966; Email: tingfan@scut.edu.cn

**Yongfei Ji** − *School of Chemistry and Chemical Engineering, Guangzhou University, Guangzhou 510006, P. R. China;* orcid.org/0000-0002-6759-7126; Email: yongfeiji2018@gzhu.edu.cn

### Authors

**Yuanyi Feng** − *School of Chemistry and Chemical Engineering, South China University of Technology, Guangzhou 510641, P. R. China*

**Mingying Sun** − *School of Chemistry and Chemical Engineering, South China University of Technology, Guangzhou 510641, P. R. China*

Complete contact information is available at: https://pubs.acs.org/10.1021/acsomega.4c00093


### Notes

The authors declare no competing financial interest.

## ACKNOWLEDGMENTS

This work is supported by the National Natural Science Foundation of China (22273024), the Natural Science Foundation of Guangdong Province (2023A1515010051 and 2023A1515012238), the Funding by Science and Technology Projects in Guangzhou (202201010374 and 202201010612), and the Guangzhou Municipal Science and Technology Bureau (202201020145). The authors gratefully acknowledge HZWTEHC for providing computation facilities.

## REFERENCES


(1) Yang, X.-F.; Wang, A.; Qiao, B.; Li, J.; Liu, J.; Zhang, T. Single-Atom Catalysts: A New Frontier in Heterogeneous Catalysis. *Acc. Chem. Res.* **2013**, *46* (8), 1740−1748, DOI: 10.1021/ar300361m.

(2) Chen, Z. W.; Chen, L. X.; Yang, C. C.; Jiang, Q. Atomic (single, double, and triple atoms) catalysis: frontiers, opportunities, and challenges. *J. Mater. Chem. A* **2019**, *7* (8), 3492−3515.

(3) Zhang, C.; Li, Y. Graphdiyne Based Atomic Catalyst: an Emerging Star for Energy Conversion. *Chem. Res. Chin. Univ.* **2021**, *37* (6), 1149−1157.

(4) Li, Y.; Xu, L.; Liu, H.; Li, Y. Graphdiyne and graphyne: from theoretical predictions to practical construction. *Chem. Soc. Rev.* **2014**, *43* (8), 2572−2586, DOI: 10.1039/c3cs60388a.

(5) He, T.; Matta, S. K.; Will, G.; Du, A. Transition-Metal Single Atoms Anchored on Graphdiyne as High-Efficiency Electrocatalysts for Water Splitting and Oxygen Reduction. *Small Methods* **2019**, *3* (9), No. 1800419, DOI: 10.1002/smtd.201800419.

(6) Ma, D.; Zeng, Z.; Liu, L.; Huang, X.; Jia, Y. Computational Evaluation of Electrocatalytic Nitrogen Reduction on TM Single-, Double-, and Triple-Atom Catalysts (TM = Mn, Fe, Co, Ni) Based on Graphdiyne Monolayers. *J. Phys. Chem. C* **2019**, *123* (31), 19066−19076.

(7) Ru, S.; He, M.; Zhou, Y.; Xu, C.; Luo, Q.; Yang, J. Theoretical and Comparative Analysis of Graphdiyne and Confined Flexible Nitrogen-Doped Graphdiyne-Supported Single-Atom Catalysts for Electrochemical Nitrogen Reduction. *J. Phys. Chem. C* **2022**, *126* (43), 18282−18291.

(8) Liu, X.; Wang, Z.; Tian, Y.; Zhao, J. Graphdiyne-Supported Single Iron Atom: A Promising Electrocatalyst for Carbon Dioxide Electroreduction into Methane and Ethanol. *J. Phys. Chem. C* **2020**, *124* (6), 3722−3730.

(9) Xue, Y.; Huang, B.; Yi, Y.; Guo, Y.; Zuo, Z.; Li, Y.; Jia, Z.; Liu, H.; Li, Y. Anchoring zero valence single atoms of nickel and iron on graphdiyne for hydrogen evolution. *Nat. Commun.* **2018**, *9* (1), No. 1460, DOI: 10.1038/s41467-018-03896-4.

(10) Lan, W.; Hu, R.; Huang, D.; Dong, X.; Shen, G.; Chang, S.; Dai, D. Palladium Nanoparticles/Graphdiyne Oxide Nanocomposite with Excellent Peroxidase-like Activity and Its Application for Glutathione Detection. *Chem. Res. Chin. Univ.* **2022**, *38* (2), 529−534.

(11) Du, Y.; Zheng, X.; Xue, Y.; Li, Y. Bismuth/Graphdiyne Heterostructure for Electrocatalytic Conversion of CO2 to Formate. *Chem. Res. Chin. Univ.* **2022**, *38* (6), 1380−1386.

(12) Rong, X.; Lu, X.; Lu, T. Three-dimensional Pyrenyl Graphdiyne Supported Pd Nanoparticle as an Efficient and Easily Recyclable Catalyst for Reduction of 4-Nitrophenol. *Chem. Res. Chin. Univ.* **2021**, *37* (6), 1296−1300.

(13) Zhao, Y.; Wan, J.; Yao, H.; Zhang, L.; Lin, K.; Wang, L.; Yang, N.; Liu, D.; Song, L.; Zhu, J.; Gu, L.; Liu, L.; Zhao, H.; Li, Y.; Wang, D. Few-layer graphdiyne doped with sp-hybridized nitrogen atoms at acetylenic sites for oxygen reduction electrocatalysis. *Nat. Chem.* **2018**, *10* (9), 924−931.

(14) Gao, Y.; Cai, Z.; Wu, X.; Lv, Z.; Wu, P.; Cai, C. Graphdiyne-Supported Single-Atom-Sized Fe Catalysts for the Oxygen Reduction Reaction: DFT Predictions and Experimental Validations. *ACS Catal.* **2018**, *8* (11), 10364−10374.

(15) Si, W.; Yang, Z.; Wang, X.; Lv, Q.; Zhao, F.; Li, X.; He, J.; Long, Y.; Gao, J.; Huang, C. Fe,N-Codoped Graphdiyne Displaying Efficient Oxygen Reduction Reaction Activity. *ChemSusChem* **2019**, *12* (1), 173−178.

(16) Li, M.; Lv, Q.; Si, W.; Hou, Z.; Huang, C. Sp-Hybridized Nitrogen as New Anchoring Sites of Iron Single Atoms to Boost the

Oxygen Reduction Reaction. *Angew. Chem., Int. Ed.* **2022**, *61* (38), No. e202208238, DOI: 10.1002/anie.202208238.
(17) Zitolo, A.; Goellner, V.; Armel, V.; Sougrati, M.-T.; Mineva, T.; Stievano, L.; Fonda, E.; Jaouen, F. Identification of catalytic sites for oxygen reduction in iron- and nitrogen-doped graphene materials. *Nat. Mater.* **2015**, *14* (9), 937−942.
(18) Kang, B.; Wu, S.; Ma, J.; Ai, H.; Lee, J. Y. Synergy of sp-N and sp2-N codoping endows graphdiyne with comparable oxygen reduction reaction performance to Pt. *Nanoscale* **2019**, *11* (35), 16599−16605.
(19) Liu, B.; Zhan, S.; Du, J.; Yang, X.; Zhao, Y.; Li, L.; Wan, J.; Zhao, Z. J.; Gong, J.; Yang, N.; Yu, R.; Wang, D. Revealing the Mechanism of sp-N Doping in Graphdiyne for Developing Site-Defined Metal-Free Catalysts. *Adv. Mater.* **2022**, *35* (50), No. 2206450, DOI: 10.1002/adma.202206450.
(20) He, J.; Ma, S. Y.; Zhou, P.; Zhang, C. X.; He, C.; Sun, L. Z. Magnetic Properties of Single Transition-Metal Atom Absorbed Graphdiyne and Graphyne Sheet from DFT+U Calculations. *J. Phys. Chem. C* **2012**, *116* (50), 26313−26321.
(21) Qin, M.; Meng, X.; Wang, W. Analysis on the secondary active site of FeN4-graphene for oxygen reduction reaction by DFT calculation. *Chem. Phys. Lett.* **2021**, *765*, No. 138321, DOI: 10.1016/j.cplett.2021.138321.
(22) Kresse, G.; Furthmüller, J. Efficiency of ab-initio total energy calculations for metals and semiconductors using a plane-wave basis set. *Comput. Mater. Sci.* **1996**, *6* (1), 15−50.
(23) Vanderbilt, D. Soft self-consistent pseudopotentials in a generalized eigenvalue formalism. *Phys. Rev. B* **1990**, *41* (11), 7892−7895.
(24) Wang, X.; Hu, X.; Zheng, L.; Lv, Q.; He, J.; Li, X.; Li, R.; Lu, T.; Huang, C. The synthesis of MNC5 active site for electrochemical catalysis. *Nano Energy* **2023**, *117*, No. 108919, DOI: 10.1016/j.nanoen.2023.108919.
(25) Lv, Q.; Li, M.; Li, X.; Yan, X.; Hou, Z.; Huang, C. Introducing hydroxyl groups to tailor the d-band center of Ir atom through side anchoring for boosted ORR and HER. *J. Energy Chem.* **2024**, *90*, 144−151.
(26) Viswanathan, V.; Hansen, H. A.; Rossmeisl, J.; Nørskov, J. K. Universality in Oxygen Reduction Electrocatalysis on Metal Surfaces. *ACS Catal.* **2012**, *2* (8), 1654−1660.
(27) Zhang, Q.; Mamtani, K.; Jain, D.; Ozkan, U.; Asthagiri, A. CO Poisoning Effects on FeNC and CNx ORR Catalysts: A Combined Experimental−Computational Study. *J. Phys. Chem. C* **2016**, *120* (28), 15173−15184.
(28) Blöchl, P. E. Projector augmented-wave method. *Phys. Rev. B* **1994**, *50* (24), 17953−17979.
(29) Gu, J.; Magagula, S.; Zhao, J.; Chen, Z. Boosting ORR/OER Activity of Graphdiyne by Simple Heteroatom Doping. *Small Methods* **2019**, *3* (9), No. 1800550, DOI: 10.1002/smtd.201800550.
(30) Zou, L.; Zhu, Y.; Cen, W.; Jiang, X.; Chu, W. N-doping in graphdiyne on embedding of metals and its effect in catalysis. *Appl. Surf. Sci.* **2021**, *557*, No. 149815, DOI: 10.1016/j.apsusc.2021.149815.
(31) Kropp, T.; Mavrikakis, M. Transition Metal Atoms Embedded in Graphene: How Nitrogen Doping Increases CO Oxidation Activity. *ACS Catal.* **2019**, *9* (8), 6864−6868.
(32) Lv, Q.; Si, W.; Yang, Z.; Wang, N.; Tu, Z.; Yi, Y.; Huang, C.; Jiang, L.; Zhang, M.; He, J.; Long, Y. Nitrogen-Doped Porous Graphdiyne: A Highly Efficient Metal-Free Electrocatalyst for Oxygen Reduction Reaction. *ACS Appl. Mater. Interfaces* **2017**, *9* (35), 29744−29752.
(33) Xiao, M.; Gao, L.; Wang, Y.; Wang, X.; Zhu, J.; Jin, Z.; Liu, C.; Chen, H.; Li, G.; Ge, J.; He, Q.; Wu, Z.; Chen, Z.; Xing, W. Engineering Energy Level of Metal Center: Ru Single-Atom Site for Efficient and Durable Oxygen Reduction Catalysis. *J. Am. Chem. Soc.* **2019**, *141* (50), 19800−19806.
(34) Lian, K.; Wan, Q.; Jiang, R.; Lin, S. Electrocatalytic Oxygen Reduction to Hydrogen Peroxide on Graphdiyne-Based Single-Atom Catalysts: First-Principles Studies. *Catalysts* **2023**, *13* (2), No. 307, DOI: 10.3390/catal13020307.
(35) Pedregosa, F.; Varoquaux, G.; Gramfort, A.; Michel, V.; Thirion, B.; et al. Scikit-learn: Machine learning in Python. *J. Mach. Learn. Res.* **2011**, *12*, 2825−2830.
(36) Friedman, J. H. Stochastic gradient boosting. *Computat. Stat. Data Anal.* **2002**, *38*, 367−378.
(37) Li, X.; Lin, S.; Yan, T.; Wang, Z.; Cai, Q.; Zhao, J. Machine-learning-accelerated screening of single metal atoms anchored on MnPS3 monolayers as promising bifunctional oxygen electrocatalysts. *Nanoscale* **2023**, *15* (27), 11616−11624.
(38) Wan, X.; Yu, W.; Niu, H.; Wang, X.; Zhang, Z.; Guo, Y. Revealing the oxygen Reduction/Evolution reaction activity origin of Carbon-Nitride-Related Single-Atom catalysts: Quantum chemistry in artificial intelligence. *Chem. Eng. J.* **2022**, *440*, No. 135946, DOI: 10.1016/j.cej.2022.135946.
(39) Jiao, D.; Zhang, D.; Wang, D.; Fan, J.; Ma, X.; Zhao, J.; Zheng, W.; Cui, X. Applying machine-learning screening of single transition metal atoms anchored on N-doped γ-graphyne for carbon monoxide electroreduction toward C1 products. *Nano Res.* **2023**, *16* (8), 11511−11520.
(40) Salem, M.; Cowan, M. J.; Mpourmpakis, G. Predicting Segregation Energy in Single Atom Alloys Using Physics and Machine Learning. *ACS Omega* **2022**, *7* (5), 4471−4481.


https://doi.org/10.1021/acsomega.4c00093
*ACS Omega* 2024, 9, 17389−17397